EFFECTS OF EPITAXIAL STRAIN ON THE GROWTH MECHANISM OF YBa$_2$Cu$_3$O$_{7-x}$ THIN FILMS IN [YBa$_2$Cu$_3$O$_{7-x}$/PrBa$_2$Cu$_3$O$_{7-x}$] SUPERLATTICES

M. Varela[a),c)], W. Grogger[b)], D. Arias[a),§], Z. Sefrioui[a)], C. León[a)], L. Vazquez[d)], C. Ballesteros[c)], K. M. Krishnan[b)], J. Santamaría[a)]

[a)] *GFMC, Dpto Física Aplicada III, Universidad Complutense, 28040 Madrid. Spain*

[b)] *Materials Sciences Division, 72-222, Lawrence Berkeley National Laboratory, University of California, Berkeley, CA 94720. U.S.A.*

[c)] *Dpto Física, Universidad Carlos III de Madrid, 28911 Leganés, Madrid. Spain*

[d)] *Instituto de Ciencia de Materiales ICMM-CSIC, 28049 Madrid. Spain*

[§] *On leave from Universidad del Quindio. Armenia. Colombia*

(February 27th 2002)

arXiv:cond-mat/0209348v1 16 Sep 2002

Abstract

We report on the growth mechanism of $YBa_2Cu_3O_{7-x}$. Our study is based on the analysis of ultrathin, $YBa_2Cu_3O_{7-x}$ layers in c-axis oriented $YBa_2Cu_3O_{7-x}$ / $PrBa_2Cu_3O_7$ superlattices. We have found that the release of epitaxial strain in very thin YBCO layers triggers a change in the dimensionality of the growth mode. Ultrathin, epitaxially strained, YBCO layers with thickness below 3 unit cells grow in a block by block two dimensional mode coherent over large lateral distances. Meanwhile, when thickness increases, and the strain relaxes, layer growth turns into three dimensional, resulting in rougher layers and interfaces.

INTRODUCTION

In recent years, thin films of complex ionic oxides have played a significant role in the discovery and understanding of important new phenomena in condensed matter physics. Basic studies or important related applications in various fields like high Tc superconductivity, colossal magnetoresistance, etc, require the growth of ultrathin films with controlled composition and morphology. In this respect, the specific growth mode seriously influences the final film structure and morphology, and thus, can deeply condition its physical properties. Growth mechanisms are determined by the chemical composition, type of chemical bonding, etc, and therefore they may be intrinsically different when going from semiconductors to metals or ionic oxides. While the questions of which is the growth mechanism and which is the minimum growth unit, have been satisfactory addressed in semiconductors or metals, in the case of ionic oxides, the growth process is still not fully understood due, probably, to the complexity of the unit cell. Experiments directed to the analysis or application of the physical properties of those ultrathin layers require an accurate control of the growth process at atomic scale. In fact, many studies fail because the chemical and physical disorder at the interfaces (interdiffusion and roughness) determined by the particular growth mechanism may invalidate the conclusions obtained for ultrathin layers [1,2].

It has been reported that in the initial stages, the growth of c-axis oriented $YBa_2Cu_3O_{7-x}$ (YBCO) films takes place quite smoothly, in a two-dimensional (2D) mode [3-5]. From the analysis of superlattices with a non-integer number of $YBa_2Cu_3O_{7-x}$ cells, in a recent letter we have reported evidence for a two-dimensional block-by-block growth mechanism in which the growth units are single unit cells [6]. We use the term block-by-block in the sense that the high substrate temperature (900 ^oC) provides the necessary mass transport for complete unit cell blocks to nucleate. We showed that it is possible to obtain laterally coherent one unit cell thick layers. On the other hand a three- dimensional growth mechanism around screw dislocations has been reported for thicker films, leading to a rough terrace-like surface morphology [7,8]. In fact this 3D growth has been recently shown to determine the critical current of YBCO thin films. Linear defects (edge and screw dislocations) associated to a 3D growth provide the strong pinning centres responsible for enhanced critical currents [7,8].

2

Since the growth of YBCO has been reported to take place in a 2D mode for very thin films, and in a 3D mode for thicker films, the question here is what is the driving mechanism to change the growth mode from 2D to 3D. In this paper we present a consistent approach based on "ex-situ" quantitative structural and chemical characterization of epitaxially grown $YBa_2Cu_3O_{7-x}$ (YBCO) layers in c-axis oriented $YBa_2Cu_3O_{7-x}/PrBa_2Cu_3O_7$(YBCO/PBCO) superlattices. The superlattice structure is of particular interest because interface planes between YBCO and PBCO were once the growth fronts, and therefore they represent an important information source to study the growth process itself. The study of the growth modes of ultrathin layers requires a quantitative structural and chemical characterization at relevant length scales. Roughness has been analyzed by complementary reciprocal and real space techniques, x-ray diffraction (XRD) and energy filtered transmission electron microscopy (EFTEM). Combining both techniques it is possible to accurately quantify the interfacial roughness in both the growth and lateral directions [9]. We have found a correlation between the release of epitaxial strain in YBCO layers, when a certain critical thickness is attained, and the appearance of roughness in the superlattices, which increases with layer thickness and confirms a 3D-like growth in relaxed samples.

EXPERIMENTAL

High quality YBCO/PBCO superlattices grown by high pressure sputtering (3.6 mbar pure oxygen)on $SrTiO_3$ substrates at 900^oC. This technique provides a very thermalized and ordered growth at a slow rate (0.013 nm/s for YBCO), which allows a very accurate control of layer thickness [10]. The films for this study were $[YBCO_n/PBCO_5]_{1000\mathring{A}}$ superlattices with nominal values for YBCO layer thickness n comprised between 1 and 12 unit cells up to a total thickness of 1000 Å. θ-2θ x-ray spectra were obtained in a conventional diffractometer using CuKα radiation. High angle XRD spectra were analysed using the SUPREX9 software, which allows obtaining quantitative values for interface disorder parameters like interdiffusion or roughness [11]. Energy-Filtered Transmission Electron Microscopy (EFTEM) investigations were performed on cross-section samples on a Philips CM200/FEG equipped with a field emission source and a post-column energy-filter (Gatan Imaging Filter, GIF). For imaging we used the low energy edges of Y and Pr, applying the two-window technique (jump ratio images, i.e., division of an image located right on the ionization edge by an image acquired before the edge onset) [12-15]. In this manner individual unit cells of YBCO and PBCO in the growth direction were resolved, and individual atomic planes of Y and Pr were detected.

RESULTS AND DISCUSSION

A set of element-specific energy filtered images, using the characteristic $Pr.N_{4,5}$ionization edge, is shown in figure 1. The darkest contrast corresponds to YBCO layers, while the

lightest contrast corresponds to PBCO layers. Energy filtered images using the characteristic Y-M $_{4,5}$ energy edge give complementary images to the ones obtained with Pr mapping [6].The images correspond to a $[YBCO_2/PBCO_5]_{1000\AA}$ (fig 1(a)) and a $[YBCO_8/PBCO_5]_{1000\AA}$ (fig 1(b)) superlattices. Magnification of the images is low, in order to get enough structural information over wide lateral scales, larger than sample thickness. While for the ultrathin YBCO layers (fig 1(a)) perfectly smooth layers of uniform thickness can be observed over long lateral distances, clear layer undulations can be observed in the thicker YBCO films of the $[YBCO_8/PBCO_5]$ superlattice (fig1(b)), resulting from thickness fluctuations with lateral length scales typically comparable to sample thickness. These images can be statistically treated to quantify roughness. Images have been digitized to find the locii of the midpoint of Y in each bilayer thus providing a lateral height profile of the individual bilayers. The standard deviation of the height distribution for each bilayer (bilayer roughness $\sigma_{bilayer}$ hereafter) can be used to examine roughness evolution along the growth direction. Alternatively the height differences between Y profiles for consecutive bilayers at the same lateral coordinate provide a map of the fluctuations in the modulation length, Λ, with $\Lambda = N_A c_A + N_B c_B$, where c_A, c_B, N_A, and N_B are the lattice parameters and number of unit cells of materials A and B, respectively. The standard deviation of the distribution of modulation lengths, σ, can be used as a measure of step disorder roughness in superlattices. Obviously the two quantities σ and $\sigma_{bilayer}$ will be different if roughness is vertically correlated. This method has been proposed recently and satisfactory applied to analyse interface roughness in Fe/Cr superlattices [9]. Histogram plots of the modulation length distributions are shown in figures 2(a) and 2(b) respectively for the $[YBCO_2/PBCO_5]_{1000\AA}$ and $[YBCO_8/PBCO_5]_{1000\AA}$ superlattices of figure 1. As depicted in 2(a) for the $[YBCO_2/PBCO_5]_{1000\AA}$ superlattice a quite sharp-peaked distribution centered in 81Å is obtained for Λ, with a standard deviation of less than 1 Å. However, the same analysis performed on the $[YBCO_8/PBCO_5]_{1000\AA}$ sample, in figure 2(b), shows a gaussian-like distribution of data around a mean value of 151 Å with a standard deviation of 6 Å. It is important to note that, the average value of the modulation length over the superlattice stacking was in agreement with the nominal overall composition of the superlattice. This shows that thickness fluctuations occur locally as a consequence of the growth process and do not result of uncontrolled fluctuations in the deposition rate. Roughness of each bilayer $\sigma_{bilayer}$ has been obtained from the standard deviation of the height distribution for each bilayer in the $[YBCO_8/PBCO_5]_{1000\AA}$ superlattice. Figure 3 shows the bilayer roughness as a function of the bilayer index in the stacking. From the observation of figure 3 one can see how the roughness increases cumulatively with bilayer index. The dotted line in figure 3 is a fit to a power law of the form, $\sigma_{bilayer} = \sigma_a N^\alpha$, being $\sigma_a = 5.2$ Å the roughness in the first bilayer, $\alpha = 0.51$ an exponent which accounts for the cumulative roughness evolution, and N is the bilayer index [9,16]. No fluctuations were found in the height distribution of each bilayer in the $[YBCO_2/PBCO_5]_{1000\AA}$ superlattice within the lateral size of the images.

Figure 4 shows the XRD spectra of a $[YBCO_1/PBCO_5]$ sample (bottom) and a $[YBCO_8/PBCO_5]$ superlattice (top), displaced vertically for clarity. XRD spectra of the $[YBCO_1/PBCO_5]$ sample show sharp superlattice satellite peaks around the main Bragg peaks, indicating a good structural quality. X ray data were analysed with the SUPREX code [11]. Lines in figure 4 are the refinement calculations supplied by the SUPREX pro-

gram. The structural model used in the refinement calculation refines thicknesses of the individual layers, c-lattice parameters and interface disorder related parameters. Interface roughness is accounted for by allowing the bilayer thickness (modulation length) to fluctuate around a mean value in a gaussian way [11]. Interface roughness compares with the standard deviation (σ) of the gaussian layer thickness distribution obtained from the EFTEM analysis. The analysis of the XRD spectra of samples with thin (1-3 unit cells) YBCO layers did not show measurable interface roughness. On the other hand, YBCO layers with thickness above 4 unit cells, show clear damping of the high order satellite peaks as a result of enhanced structural disorder, (see figure 4). In this case the structural refinement confirms the presence of random layer thickness fluctuations which increases with YBCO layer thickness (see figure 5(a)). Good agreement was found between roughness values obtained from XRD and from electron microscopy. The roughness parameter σ=8 Å obtained from x-rays for the [YBCO$_8$/PBCO$_5$] superlattice has to be compared with the standard deviation of the distribution of modulation lengths (6 Å) obtained from the electron microscopy analysis. We have previously shown that superlattices with YBCO layer thickness below 4 unit cells grow epitaxially strained due to lattice mismatch to PBCO [10,17]. Figure 5 shows the evolution of the YBCO c-lattice parameter with YBCO layer thickness. It can be observed that for YBCO thickness below 4 unit cells there is a significant contraction of the c lattice spacing arising from the 1% lattice mismatch to PBCO according to Poisson effect [17]. Interestingly, roughness increases sharply above 3 unit cells, when epitaxial strain relaxes (see figure 5). When increasing YBCO thickness over this critical value the strain relaxes, and simultaneously the superlattice interfaces become rougher. These results point to a change in the growth mechanism of YBCO from a 2D-like in epitaxially strained samples to a 3D rough growth for YBCO thickness over 4 unit cells. An interesting question is whether the 3D growth mode of the rough relaxed samples already provides the linearly correlated disorder (edge and screw dislocations) which have recently shown to effectively pin vortices in thicker (140 nm) samples [7].We have done measurements of the angular dependence of the magnetoresistance at temperatures ranging between 0.7 T$_c$ and 0.99 T$_c$, in magnetic fields ranging from 100 to 90000 gauss. No evidence was found for "cusp"- like features characteristic of vortex confinement by correlated disorder. This evidences that thicker samples are necessary for these defects to develop and /or to be effective for vortex pinning.

Attempts were done to artificially induce roughness in the *ultrathin* YBCO layers growing a non integer number of YBCO unit cells. Figure 6 shows an element-specific energy-filtered images, using the characteristic Pr-N$_{4,5}$ edge for a [YBCO$_{1.5}$/PBCO$_5$] superlattice. Lattice fringes are observed, though this contrast is not element specific. The superlattice, with a non-integer number of unit cells of YBCO in the stack, shows abrupt changes in the YBCO layer thickness from one to two unit cells, through steps one unit cell high, over a lateral length scale ranging from 100-200 nm. The specimen thickness in the direction parallel to the electron beam is of the order of 10-30 nm, well below the lateral dimension where a film of uniform thickness can be grown. In this incommensurate superlattices, layer discontinuities and interface steps are observed, leading to non-smooth interfaces, but the spatial distribution of such defects seems to be non random.

Low angle ($2\theta \leq 10^o$) x-ray diffraction spectra of a set of [YBCO$_n$/PBCO$_5$] superlattices with n ranging between 1 and 2 YBCO unit cells are shown in figure 7. In this angular range,

x rays are not sensitive to crystal structure, but to the chemical modulation, and due to the x-ray grazing incidence the spectra provide information averaged over large areas of the sample. From bottom to top the spectra depicted correspond to n=1.2, 1.5 and 2 YBCO unit cells. Finite size oscillations corresponding to sample thickness can be detected, denoting a flat sample surface. Low angle superlattice peaks, labeled by m, and sharp satellite peaks, corresponding to the first superlattice Bragg peak (denoted by n) are also observed. Low angle peaks are determined by the modulation length, Λ. Superlattice Bragg peaks are determined by the average lattice spacing c= $\Lambda/(N_A+N_B)$. Satellite peaks corresponding to the first Bragg peak will occur for q vectors given by q=2π /c - 2$\pi l/\Lambda$, where l are integers. Thus, if the modulation length is a non-integer number times the average lattice spacing, low angle peaks and satellites from the first Bragg peak will not merge [18]. Moreover, in the presence of step-disorder the non-integer modulation arises from a layer thickness fluctuation around a mean value, with a standard deviation quantifying the step-disorder roughness. This randomness causes satellite broadening and overshadows the apparent splitting in most cases. However, the analysis of the XRD patterns for integer number of YBCO layers has shown the absence of step-disorder in our superlattices [10]. Hence, in the absence of step-disorder, the layer thickness does not fluctuate in a random fashion, and an unusual superlattice diffraction pattern arises with sharp diffraction satellite peaks. Such a splitting in satellite orders is noticeable in figure 7 confirming that composition changes coherently from interface plane to interface plane. A similar behaviour has been previously observed in MBE grown semiconductor superlattices [18] and also in complex oxide superlattices [6,19]. These x-ray scattering results provide strong evidence for a lateral growth mode in which the growth units are complete YBCO units cells, i.e. a 2D block-by-block growth mechanism and layer growth would take place by the lateral deposition of blocks one unit cell in height [6,20]. The composition of the interface plane is observed to change coherently from one bilayer to the next one as a result of a coherent 2D layer growth [18]. The coherent 2D growth of strained layers minimize the interface energy at the cost of the excess of elastic energy due to lattice mismatch. Increasing YBCO thickness relaxes stored elastic energy, and triggers a change to a 3D growth mode which results in terrace-like and spiral growth. Figure 8 shows an atomic force microscopy (AFM) image of a thick (300 Å) YBCO film on a 5 u.c. PBCO buffer, showing a distribution of pyramid structures. Terraces are 250 nm wide and steps between terraces of the height of one u.c. are observed. This clearly shows that a 3D growth mechanism is developed upon strain relaxation.

Finally, it is interesting to compare the results obtained for the growth of YBCO in YBCO/PBCO superlattices with the growth of single YBCO layers [21,22]. Thin YBCO layers were grown on single STO substrates (100) oriented. Layer thickness was determined from low angle x-ray reflectivity oscillations. For YBCO layer thickness below 10 nm a significant c lattice contraction is observed (see figure 9 (a)), which correlates with a substantial reduction of the critical temperature (see figure 9 (b)). Critical temperatures are evaluated at zero resistivity. It is important to note that critical temperatures in excess of 80 K are practically recovered for YBCO thickness larger than 10 nm. This results are consistent with recent calculations which propose a critical thickness of YBCO on STO of 80 nm [23]. Note that despite a larger lattice mismatch with STO (-1.4% and -0.7 % along a and b axis respectively) than with PBCO (-0.7 % and -1.1 % along a and b axis respectively) the critical thickness is larger for films grown on STO. This can be discussed from two different

viewpoints.On the one hand the superlattice geometry in which the YBCO layers are sandwiched between PBCO layers stresses YBCO more efficiently. This method would probably underestimate the critical thickness of single films grown on PBCO buffer layers. On the other hand, and probably more important, ultrathin layers are very delicate and exposure to ambient atmosphere can chemically affect the surface and degrade the superconducting properties. We want to remark that these results may also depend on growth parameters and deposition technique. Substantially different results have been recently reported [8] for films of comparable thickness grown by pulsed laser deposition (PLD) at significantly lower growth temperatures (770-850 ^oC) than in this work (900 ^oC). Reference [8] shows an increase of the c-lattice parameter when the YBCO is reduced, contrary to the expectations of Poisson effect.

In summary, we have shown that strained ultrathin YBCO layers on PBCO grow in a two-dimensional block-by-block mode, where the minimum growth unit is a whole oxide unit cell. Layer grows laterally by the successive deposition of one unit cell blocks "wetting" the surface. When increasing YBCO layer thickness over 3-4 unit cells epitaxial strain relaxes, and random interface roughness arises which increases cumulatively with YBCO layer thickness. Strain relaxation triggers a change in the growth mode from 2D to 3D. This 3D growth mode in thick YBCO layers is in agreement with previous observations of growth pyramids, with steps one unit cell high, in thick YBCO layers.

I.

ACKNOWLEDGMENTS

REFERENCES

[1] E. E. Fullerton, J. Guimpel, O. Nakamura, I. K. Schuller, Phys. Rev. Lett **69**, 2859 (1992).

[2] I. N. Chan, D.C. Vier, O. Nakamura, J. Hasen, J. Guimpel, S. Schultz , I.K. Schuller, Phys. Lett. A **175**, 241 (1993).

[3] C. L. Jia, H. Soltner, G. Jacob, T. Hahn, H. Adrian, K. Urban. Physica **C 210**, 1 (1993).

[4] S. J. Pennycook, M. F. Chisholm, D. E. Jesson, D. P. Norton, D. H. Lowndes, R. Feenstra, and H. R. Kerchner, J. O. Thomson. Phys. Rev. Lett. **67**, 765 (1991).

[5] T. Terashima, Y. Bando, K. Iijima, K. Yamamoto, K. Hirata, K. Hayashi, K. Kamigaki, and H. Terauchi. Phys. Rev. Lett. **67**, 1362 (1991)

[6] M. Varela, W. Grogger, D. Arias, Z. Sefrioui, C. León, C. Ballesteros, K. M. Krishnan, J. Santamaría. Phys. Rev. Lett. **86**, 5156 (2001).

[7] B. Dam, J. M. Huijbregtse, F. C. KLaassenk, R. C. F. Van der Geest, G. Doornbos,J. H. Rector, A. M. Testa, S. Freisem, J. C. Martinez, B. Stäuble-Pümpin &R. Griessen, Nature **399**, 439 (1999)

[8] B. Dam, J. M. Huijbregtse, and J. H. Rector, Phys. Rev. B **65**, 064528 (2002)

[9] M.C. Cyrille, S. Kim, M.E. Gómez, J. Santamaría, K.M. Krishnan and I.K. Schuller. Phys. Rev. B **62**, 3361 (2000)

[10] M. Varela, D. Arias, Z. Sefrioui, C. León, C. Ballesteros, J. Santamaría. Phys. Rev. B. **62** 12509 (2000).

[11] E. E. Fullerton, I. K. Schuller, H. Vanderstraeten, Y. Bruynseraede, Phys. Rev. B **45**, 9292 (1992).

[12] O. L. Krivanek, M. K. Kundmann, K. Kimoto, J. Microsc. **180** 277 (1995).

[13] F. Hofer, W. Grogger, G. Kothleitner, P. Warbichler, Ultramicroscopy **67**, 83 (1997).

[14] T. Navidi-Kasmai, H. Kohl, Ultramicroscopy **81**, 223 (2000).

[15] O. L. Krivanek, A. J. Gubbens, M. K. Kundmann, G. C. Carpenter, Proc. 51st Annual Meeting Microsc. Soc. Am., eds. G. W. Bailey \& C. L. Rieder (San Francisco Press, San Francisco), 586 (1993).

[16] A.L. Barabasi, H.E. Stanley. Fractal concepts in surface growth. Cambridge Univ. Press (1995)

[17] M. Varela, Z. Sefrioui , D. Arias, M. A. Navacerrada, M. Lucía, M. A. López de la Torre, C. León, G. Loos, F. Sánchez-Quesada and J. Santamaría. Phys. Rev. Lett. **83** 3936 (1999)

[18] I. K. Schuller, M. Grimsditch, F. Chambers, G. Devane, H. Vanderstraeten, D. Neerinck, J.-P. Locquet, and Y. Bruynseraede, Phys. Rev. Lett. **65**, 1235 (1990).

[19] G. Balestrino, G. Pasquini, A. Tebano. Phys.Rev.B **62** 1421 (2000)

[20] J. P. Locquet, A. Catana, E. Mächler, C. Gerber, J. G. Bednorz, Appl. Phys. Lett. **64**, 372 (1994).

[21] L. Cao and J. Zegenhagen, Phys. Stat. Sol. (b) **215**, 587 (1999)

[22] L. X. Cao, J. Zegenhagen, M. Cardona, C. Giannini, L. De Caro, and L. Tapfer, J. Appl. Phys. **91**, 1265 (2002)

[23] L. X. Cao, T. L. Lee, F. Renner, Y. Su, R. L. Johnson, and J. Zegenhagen, Phys. Rev. **B 65**, 113402 (2002)

II.

III. FIGURE CAPTIONS

Figure 1: (a) Pr-N $_{4,5}$ energy filtered image of a [YBCO$_2$/PBCO$_5$] superlattice in cross section geometry. White contrast corresponds to PBCO layers, while YBCO layers appear dark. (b) Pr-N4,5 energy filtered image of a [YBCO$_8$/PBCO$_5$] superlattice. Note the fluctuations in layer thicknesses.

Figure 2: (a) Histogram plot of the distribution of modulation lengths Λ obtained from the EFTEM images in the [YBCO$_2$ /PBCO$_5$] superlattice. The dotted line is a gaussian fit, with a standard deviation of 0.7 Å (b) Histogram plot corresponding to the [YBCO$_8$/PBCO$_5$] superlattice. The gaussian curve fit shows a standard deviation of 6 Å.

Figure 3: Roughness of each bilayer versus bilayer index, N, for the [YBCO$_8$/PBCO$_5$] sample. The dotted line is a fit to a power law $\sigma=\sigma_a$ N$^\alpha$, being $\sigma_a = 5.2$ Å the roughness in the first bilayer and $\alpha =0.51$ an exponent which accounts for the roughness evolution.

Figure 4: XRD spectra (dots) together with the structural refinement (superimposed solid line) for a [YBCO$_1$/PBCO$_5$] superlattice (bottom) and a [YBCO$_8$/PBCO$_5$] sample (top). Note how high order satellites are damped in the second case.

Figure 5: (a) Step disorder roughness (σ) extracted form the XRD refinement versus YBCO layer thickness for a set of [YBCO$_n$/PBCO$_5$] superlattices with $12 \succ n \succ 1$ u.c. (b) Evolution of the YBCO c-lattice parameter with YBCO layer thickness for the same samples. When YBCO thickness increases, epitaxial strain relaxes and roughness shows up.

Figure 6: (a) Element-specific energy-filtered images, using the characteristic Pr-N $_{4,5}$ edge for a [YBCO$_{1.5}$/PBCO$_5$] superlattice in cross section geometry. White contrast corresponds to PBCO layers, while YBCO layers appear dark (b) Zoom view of figure 6(a). Interfacial steps of one unit cell are clearly observed.

Figure 7: Low angle XRD spectra for a set of [YBCO$_n$/PBCO$_5$] superlattices with non-integer YBCO layers. From bottom to top n=1.2, 1.5, and 2 YBCO unit cells. Note the splitting (marked with dotted lines) between the low angle satellite peaks and the satellites of the first Bragg peak resulting of the incommensurate modulation.

Figure 8: Atomic force microscopy (AFM) image of a thick (300 Å) YBCO film on a 5 u.c. PBCO buffer, showing a distribution of pyramid structures. Terraces are 250 nm wide. Steps between terraces of the height of one unit cell (11.7 Å) are observed.
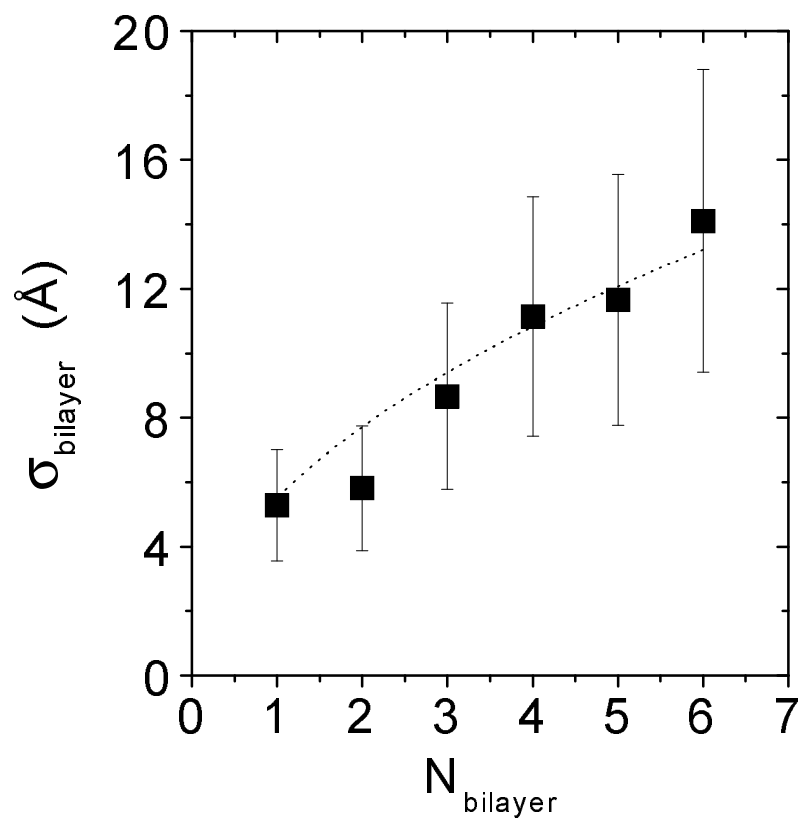
Figure 9: c-lattice parameter (a) and critical temperature (b) as a function of YBCO thickness for films grown on STO (100). Lines are guides for the eye.
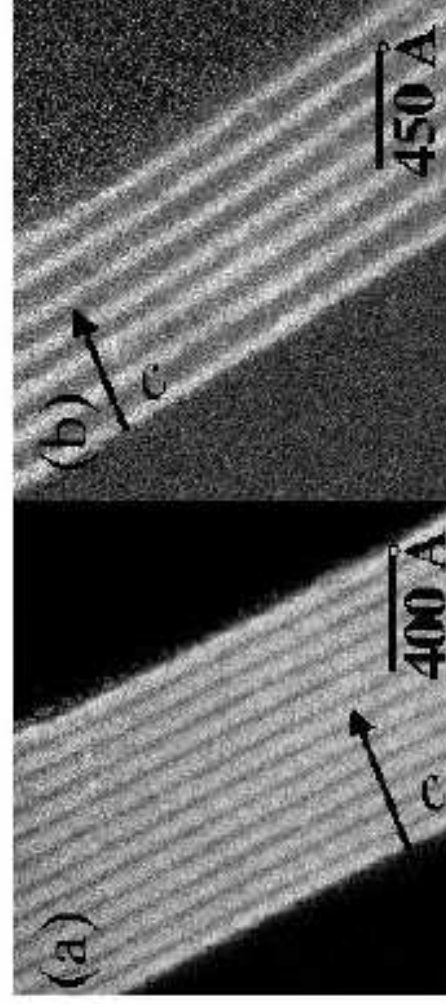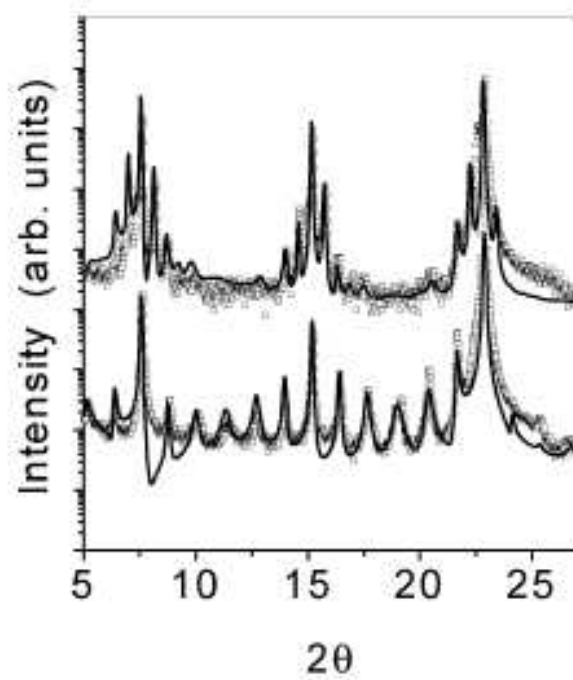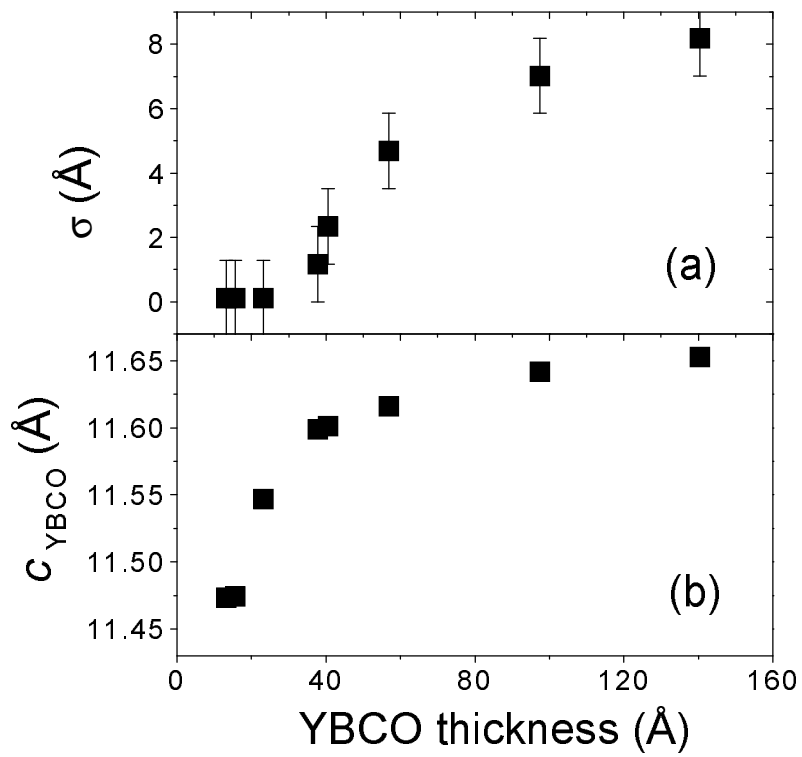
M. Varela *et al*
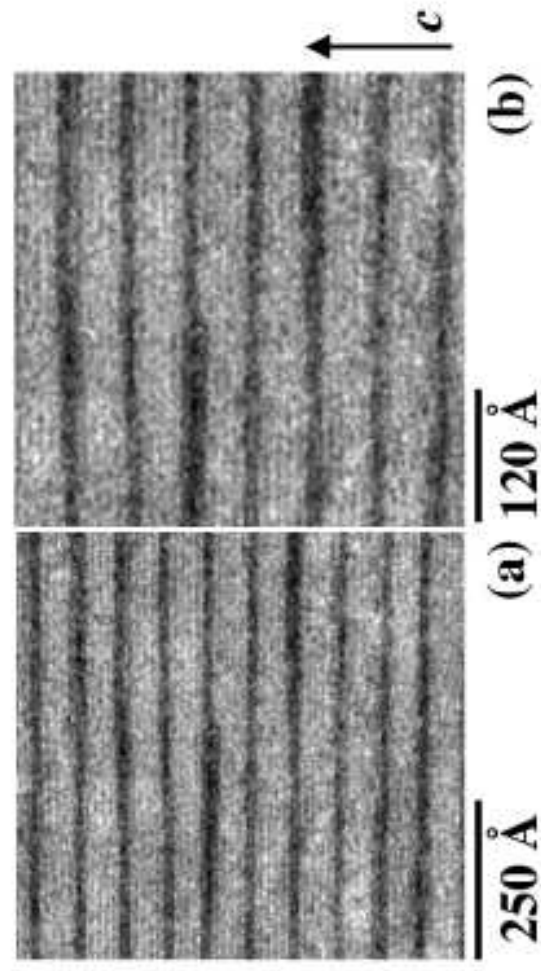Figure 1
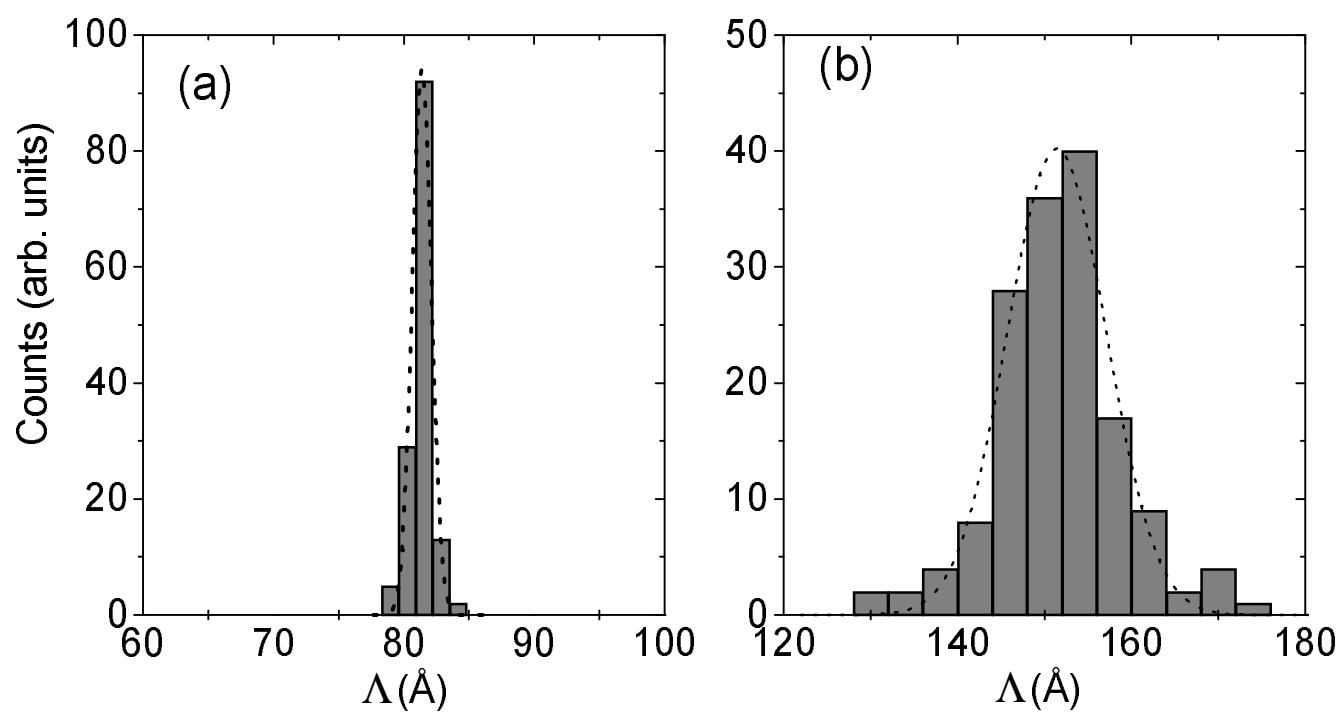
M. Varela et al.
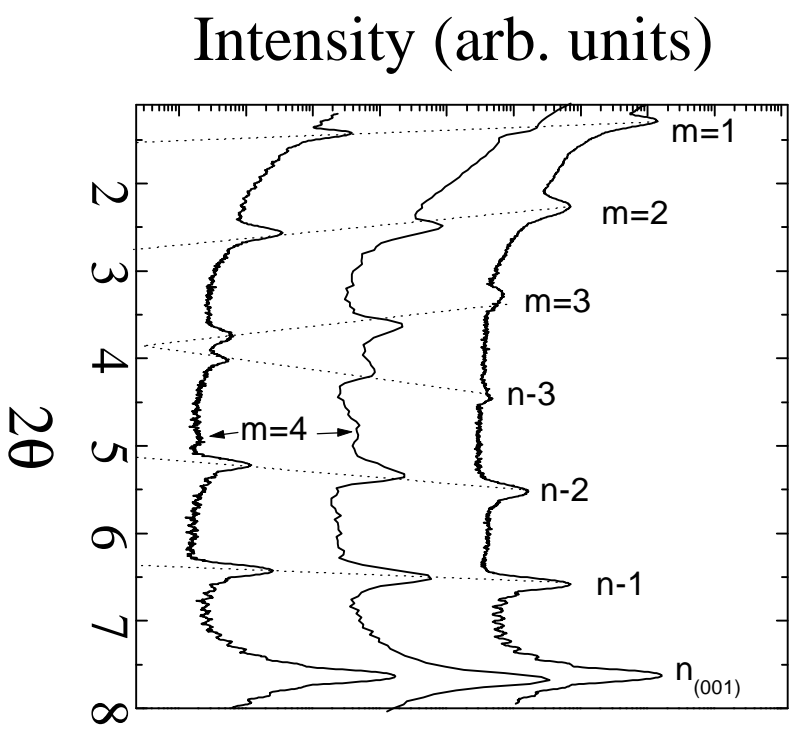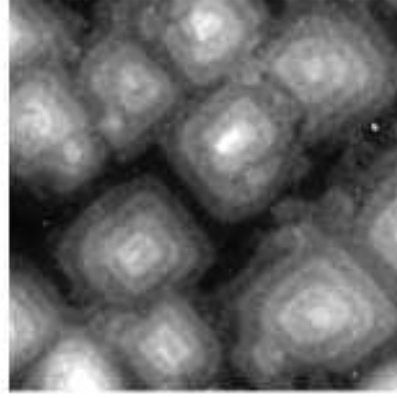Figure 2

M. Varela et al
Figure 3

M. Varela et al

Figure 4

M. Varela et al
Figure 5

(a) 250 Å (b) 120 Å

c

M. Varela et al
Figure 6

Intensity (arb. units)

m=1
m=2
m=3
n-3
m=4
n-2
n-1
n
(001)

2θ

2 3 4 5 6 7 8

M. Varela et al
Figure 7

2500Å

M. Varela et al
Figure 8